© The American Society of Gene & Cell Therapy

Anti-inflammatory Therapy With Simvastatin Improves Neuroinflammation and CNS Function in a Mouse Model of Metachromatic Leukodystrophy

Axel Stein[1], Stijn Stroobants[2], Volkmar Gieselmann[1], Rudi D'Hooge[2] and Ulrich Matzner[1]

[1]*Institut für Biochemie und Molekularbiologie, Rheinische Friedrich-Wilhelms Universität, Bonn, Germany;* [2]*Laboratory of Biological Psychology, Department of Psychology, University of Leuven, Leuven, Belgium*

Metachromatic leukodystrophy (MLD) is a lysosomal storage disease caused by a functional deficiency of the lysosomal enzyme arylsulfatase A. The prevailing late-infantile variant of MLD is characterized by widespread and progressive demyelination of the central nervous system (CNS) causing death during childhood. In order to gain insight into the pathomechanism of the disease and to identify novel therapeutic targets, we analyzed neuroinflammation in two mouse models reproducing a mild, nondemyelinating, and a more severe, demyelinating, variant of MLD, respectively. Microgliosis and upregulation of cytokine/chemokine levels were clearly more pronounced in the demyelinating model. The analysis of the temporal cytokine/chemokine profiles revealed that the onset of demyelination is preceded by a sustained elevation of the macrophage inflammatory protein (MIP)-1α followed by an upregulation of MIP-1β, monocyte chemotactic protein (MCP)-1, and several interleukins. The tumor necrosis factor (TNF)-α remains unchanged. Treatment of the demyelinating mouse model with the nonsteroidal anti-inflammatory drug simvastatin reduced neuroinflammation, improved the swimming performance and ataxic gait, and retarded demyelination of the spinal cord. Our data suggest that neuroinflammation is causative for demyelination in MLD mice and that anti-inflammatory treatment might be a novel therapeutic option to improve the CNS function of MLD patients.

Received 23 December 2014; accepted 6 April 2015; advance online publication 12 May 2015. doi:10.1038/mt.2015.69

INTRODUCTION

Lysosomal storage diseases (LSDs) are a group of ~50 inherited metabolic disorders that result from defects of the lysosomal homeostasis leading to the intralysosomal accumulation of undegraded macromolecules, a severe multisystemic disease phenotype and early death.[1] Together, LSDs have an incidence of 1/7,000 newborns and therefore represent an important subgroup among genetic neurological disorders. Different organs such as the liver, spleen, bone, cartilage, and/or the nervous system can be affected. In approximately two third of the LSDs, the clinical picture is dominated by a progressive CNS disease caused by neurodegeneration or demyelination. The CNS symptoms vary between LSD entities and variants and can involve mental retardation, ataxia, seizures, dementia, deafness, and blindness.

In contrast to the diversity in lysosomal storage materials, affected cell types, and neurological symptoms, neuroinflammation appears to be a common theme of all LSDs with CNS involvement. Microgliosis and elevated levels of cytokines and chemokines have been detected in mouse models of mucopolysaccharidosis (MPS) type I,[2,3] MPS IIIA,[3] MPS IIIB,[2,3] Niemann-Pick type C,[4] GM1-gangliosidosis,[5] Sandhoff disease,[5–7] neuronopathic Gaucher disease,[8] Farber disease,[9] globoid cell leukodystrophy,[10,11] and neuronal ceroid lipofuscinosis.[12] In some of these models, *e.g.*, of Farber disease,[13] Sandhoff disease,[14] and globoid cell leukodystrophy,[15] neuroinflammation results in the recruitment of peripheral immune cells to the CNS.

Metachromatic leukodystrophy (MLD; OMIM #250100) is a LSD caused by a functional deficiency of the lysosomal enzyme arylsulfatase A (ASA; E.C. 3.1.6.8). The deficiency leads to the intralysosomal accumulation of the sphingolipid 3-O-sulfogalactosylceramide (sulfatide), demyelination of the CNS, severe neurological symptoms, and premature death.[16] Neuroinflammation has not yet been studied in MLD. To fill this gap, we made use of two MLD mouse models. Nondemyelinating ASA knockout mice develop a mild form of the disease which is reminiscent of preclinical stages of MLD.[17] The life expectancy is, however, not reduced and these mice never show progressive and widespread demyelination which is the hallmark of the human disease. ASA knockout mice which overexpress a cerebroside sulfotransferase transgene from a proteolipoprotein promoter have a more severe phenotype.[18] This is explained by an increased rate of sulfatide synthesis in myelinating cells accelerating sulfatide storage and manifestation of symptoms. The demyelinating model has a reduced life span of 18–20 months, starts to demyelinate at age 16 months and develops severe neurological symptoms including hind limb paralysis. It is, therefore, a more authentic model of the human condition and considered to recapitulate the clinical phase of MLD.

The first two authors contributed equally to this work.

Correspondence: *Ulrich Matzner, Institut für Biochemie und Molekularbiologie, Rheinische Friedrich-Wilhelms Universität, Nussallee 11, D-53115 Bonn, Germany. E-mail: matzner@uni-bonn.de*

© The American Society of Gene & Cell Therapy

In the present study, we demonstrate that both mouse models develop progressive neuroinflammation which correlates with the degree of sulfatide storage and severity of neurological symptoms. Furthermore, we provide the first *in vivo* data on an anti-inflammatory treatment approach for MLD. For this purpose, demyelinating MLD mice were fed with simvastatin, a nonsteroidal anti-inflammatory drug which has not been tested in any LSD mouse model before.

RESULTS

Design of study

Nondemyelinating and demyelinating MLD mice were studied at two ages. First, after the onset of symptoms at 12 months and second, preferably late in their disease progression. While, the normal life expectancy of nondemyelinating MLD mice allowed the second analysis at 24 months, demyelinating MLD mice were analyzed at 16–18 months due to the high mortality after the onset of myelin loss (at 16 months). For cytokine/chemokine measurements, five mice reaching an exceptional old age of 20 months were additionally included. Sulfatide storage of the relevant age groups was analyzed by thin layer chromatography (TLC). Compared with wild-type controls, mean sulfatide levels of nondemyelinating MLD mice were increased 1.3- and 1.7-fold at 12 and 24 months, respectively (**Figure 1**). For 12- and 17-month-old demyelinating MLD mice, the factors of increase were 1.8 and 2.4, respectively.

Microgliosis and astrogliosis

The brain and spinal cord of the two MLD mouse models were analyzed by immunostaining of histological sections with antibodies to F4/80 and to the glial fibrillary acidic protein, respectively. As shown for the brain stem in **Figure 2**, staining of the microglial marker F4/80 reveals an enlargment of cell somata and thickening of cellular processes, two morphological changes indicative of reactive microgliosis. In 12-month-old nondemyelinating ASA knockout mice, these histological alterations are faint and confined to the brain stem, cerebellar white matter, and corpus callosum, whereas microglial activation is clearly amplified and generalized at 24 months as well as in 12-month-old demyelinating MLD mice. Microgliosis progresses substantially until end-stage disease as shown by the advanced morphological changes in 16-month-old demyelinating MLD mice. Microglial

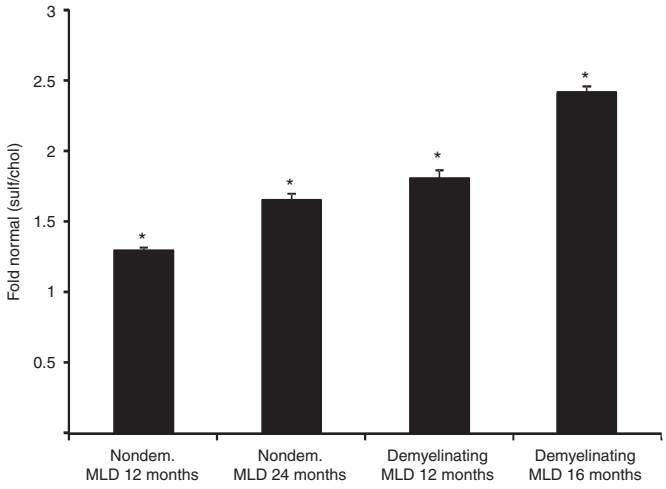

Figure 1 Sulfatide storage in brains of nondemyelinating (Nondem.) and demyelinating metachromatic leukodystrophy mice. Sulfatide of the indicated groups of mice was analyzed by TLC. Cholesterol was used as an internal standard, and the ratio between sulfatide and cholesterol (sulf/chol) was calculated. The normalized sulfatide levels are expressed as fold increase above mean levels of wild-type tissues. Bars represent means ± SEM (n = 3). Statistically significant differences to wild-type controls are indicated by asterisks (*P < 0.05).

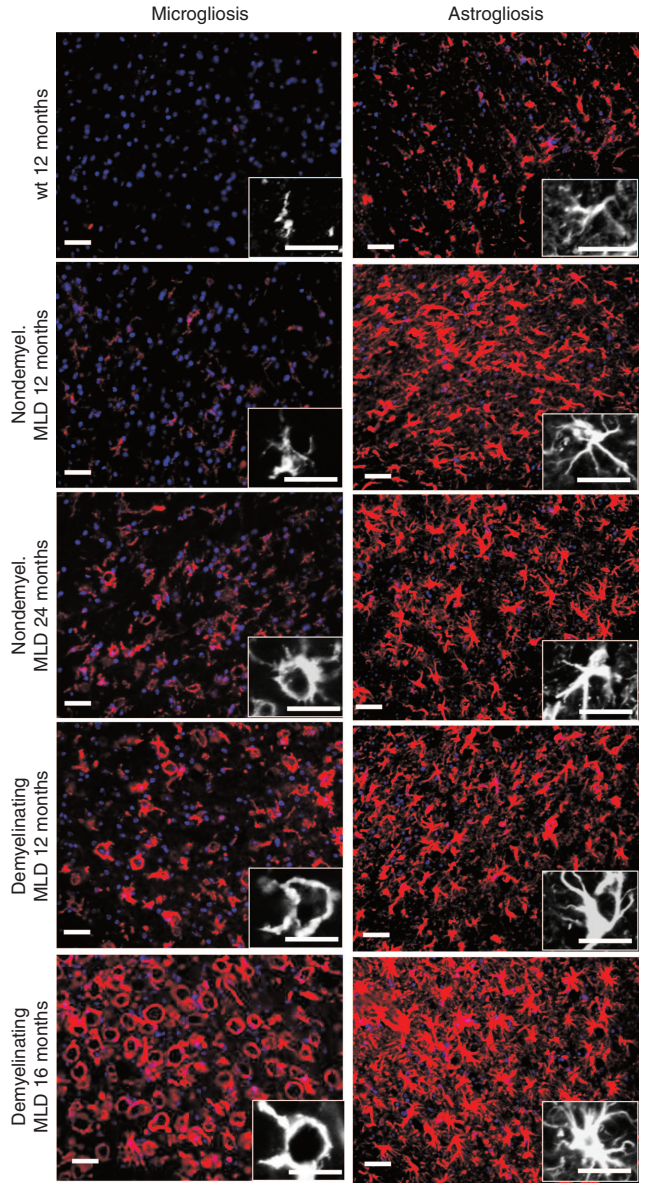

Figure 2 Microgliosis and astrogliosis in the two metachromatic leukodystrophy mouse models. Sagittal brain sections of n = 2–3 mice per group were stained with antibodies to the microglial marker protein F4/80 (left panel) and the astroglial marker protein glial fibrillary acidic protein (right panel), respectively. Nuclei were counterstained with 4′,6-diamidino-2-phenylindole. Representative immunofluorescence stainings of corresponding regions of the brain stem (medulla oblongata) are shown. Groups and ages as indicated on the left of the images. Inserts are higher power images of individual microglial and astroglial cells, respectively. Bars represent 50 µm (overviews) and 25 µm (inserts), respectively.

© The American Society of Gene & Cell Therapy

activation is paralleled by progressive astrogliosis in both animal models as indicated by an increasing number of glial fibrillary acidic protein-positive cells and the enlargement of radiating astrocytic processes particularly in the corpus callosum and other white matter tracts.

Cytokine/chemokine profiles

Cytokines/chemokines were quantified by enzyme-linked immunosorbent assay (ELISA) on whole brain homogenates. For nondemyelinating ASA knockout mice, the levels of interleukin (IL)-1β, keratinocyte chemoattractant (KC, CXCL1) and macrophage inflammatory protein (MIP)-1α (CCL3) were analyzed at age 12 and 24 months. Compared to wild-type controls, the only increase was found for MIP-1α at 24 months (**Figure 3**). Similar investigations with single-plex ELISAs revealed more complex changes of cytokines/chemokines in the demyelinating MLD mouse model (not shown). To obtain detailed information about the temporal cytokine/chemokine profile in these mice, 23 factors implicated in neuroinflammatory pathways were quantified by multi-plex ELISAs at age 10, 16, and 20 months. In contrast to the nondemyelinating model, overexpression of MIP-1α was detectable at 10 months and persisted until 20 months (**Figure 4**). The increase of other factors was temporally delayed. Monocyte chemotactic proteins (MCP)-1 (CCL2) and MIP-1β (CCL4), for example, were elevated only at 16 and 20 months. First increases of KC and RANTES (CCL5) occurred even later and were detectable at 20 months for the first time. A stage-dependent upregulation was also seen for a variety of interleukins with a transient increase of IL-1β, IL-9, IL-13, IL-17 at 16 months and sustained overexpression of IL-6 and IL-12 p40 at 16 and 20 months. During the course of the disease, the

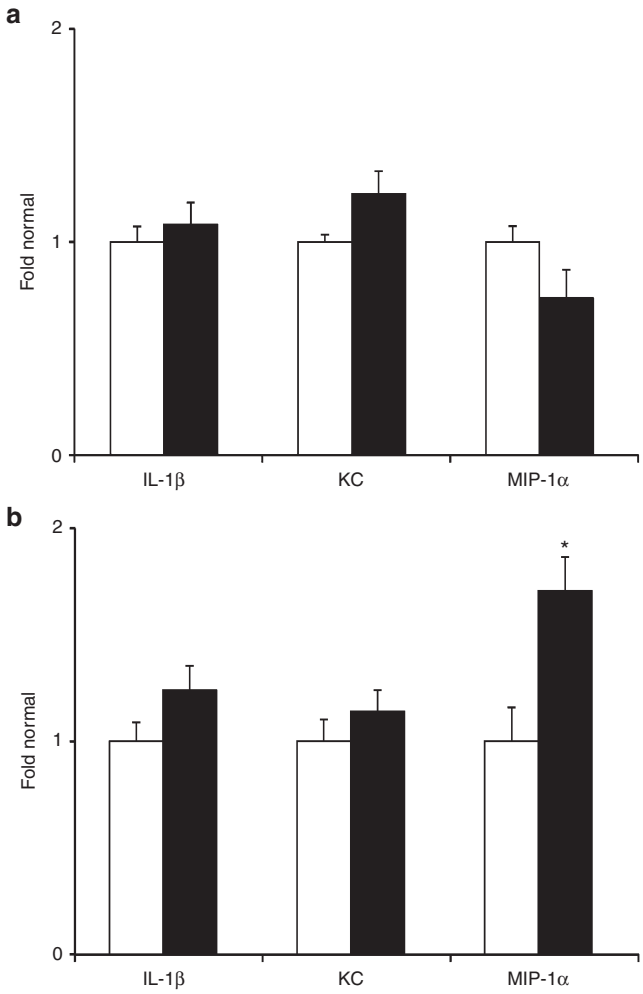

Figure 3 Brain cytokine/chemokine levels of nondemyelinating metachromatic leukodystrophy (MLD) mice. The concentration of the indicated factors was determined in ASA knockout mice (closed bars) and age-matched wild-type controls (open bars) at age (**a**) 12 and (**b**) 24 months, respectively. Cytokines levels were quantified by single-plex enzyme-linked immunosorbent assays, normalized to the protein concentration of the homogenate and expressed as multiples of the mean wild-type levels. The bars represent means ± SEM of $n = 3$ mice per group. Asterisks indicate statistically significant differences between MLD mice and controls (*$P < 0.05$).

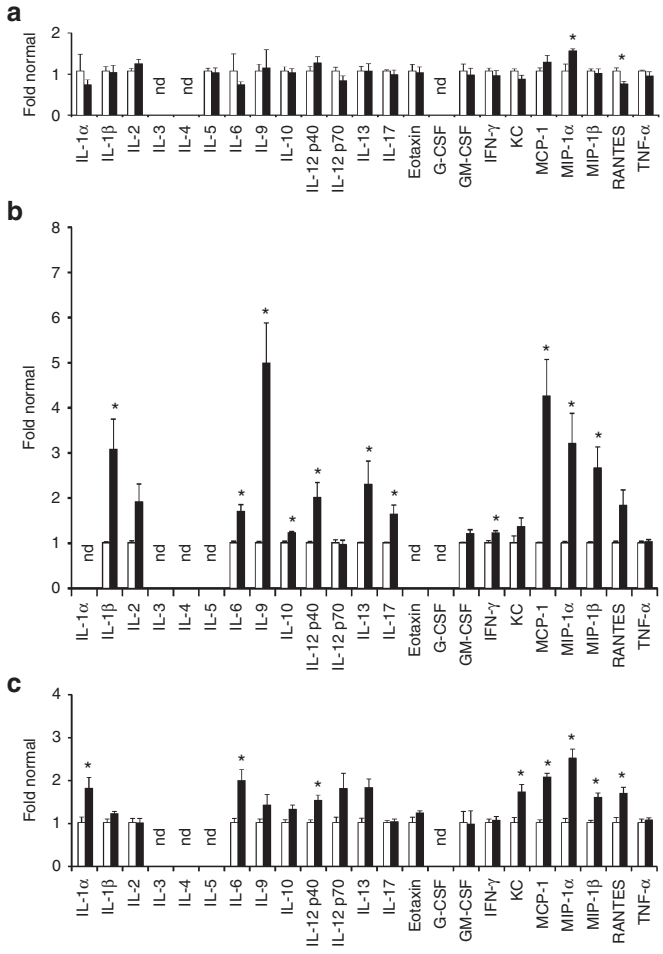

Figure 4 Brain cytokine/chemokine levels of demyelinating metachromatic leukodystrophy (MLD) mice. The concentration of the indicated 23 factors was determined in MLD mice (closed bars) and age-matched wild-type controls (open bars) at age (**a**) 10, (**b**) 16, and (**c**) 20 months, respectively. Cytokines/chemokines were quantified by multi-plex enzyme-linked immunosorbent assay, normalized to the protein concentration of the corresponding homogenate and expressed as multiples of the mean wild-type levels. The bars represent means ± SEM of $n = 3$–5 mice per group. Asterisks indicate statistically significant differences between MLD mice and controls (*$P < 0.05$). nd, not determinable.

© The American Society of Gene & Cell Therapy

overexpression was highest for IL-9 (4.9-fold), MCP-1 (4.2-fold) and MIP-1α (3.2-fold).

Infiltration of immune cells into the CNS

The function of MIP-1α, MIP-1β, and MCP-1 involves the chemoattraction of peripheral immune cells to sites of inflammation. Due to the upregulation of these factors, a possible infiltration of granulocytes, T-cells, and monocytes into the brain was investigated by immunostaining of brain sections of 17-month-old demyelinating MLD mice for cell type–specific marker proteins (Figure 5a). Staining of granulocytes with anti Ly-6G antibodies revealed prominent signals in spleen sections, stained as a control, but no signals in brain sections of MLD mice. Anti CD3ε antibodies, on the contrary, detected T-cells in the brains of demyelinating MLD mice. Immunoreactivity was specifically found in the vicinity of blood vessels, but not within the brain parenchyma indicating a perivascular localization of the infiltrated T-cells. Staining was absent from age-matched wild-type controls. Staining of the surface protein F4/80 and counterstaining of cell nuclei with 4′,6-diamidino-2-phenylindole allowed for the detection of cell somata of microglial cells and macrophages. Quantification of such somata in two brain regions (medulla oblongata, medial cerebellar nucleus) of wild-type controls and demyelinating MLD mice revealed no significant changes in the number of microglia/macrophages (shown for the medulla oblongata in Figure 5b).

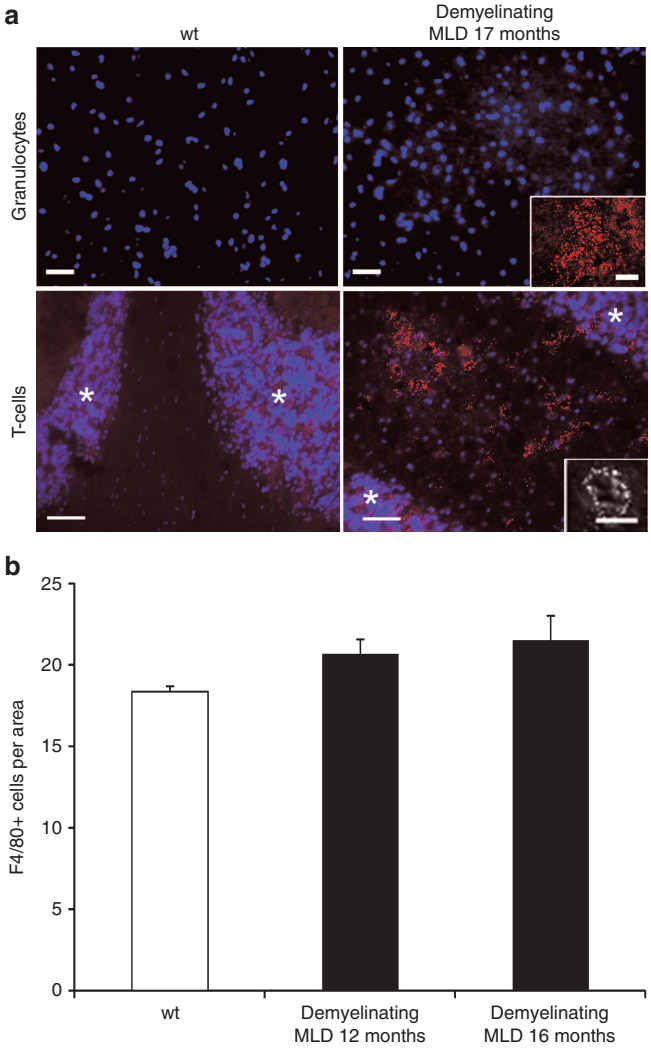

Figure 5 Infiltration of peripheral immune cells into the brain of demyelinating metachromatic leukodystrophy (MLD) mice. (**a**) Sagittal sections through the medial cerebellar nucleus of 17-month-old demyelinating MLD mice and wild-type controls were immunostained with antibodies to the granulocyte marker protein Ly-6G (upper panel; insert shows spleen section as positive control) and the pan T-cell marker protein CD3ε (lower panel; insert shows perivascular T-cells under higher magnification), respectively. Nuclei were counterstained with 4′,6-diamidino-2-phenylindole. Representative immunofluorescence images of $n = 2–3$ mice per group are shown. Bars represent 50 µm (overviews), 100 µm (insert, granulocytes), and 25 µm (insert, T-cells) respectively. The granule cell layer is indicated by asterisks. (**b**) Macrophages/microglial cells in the medulla oblongata of the indicated groups of mice. F4/80-positive nucleated profiles were counted as described in the method section. No significant differences between groups were detectable. Bars are means ± SEM of $n = 2–3$ mice per group.

Anti-inflammatory therapy

Demyelinating MLD mice were treated with 20 mg/kg/day simvastatin for 30 days. Simvastatin was tolerated by all age groups without any obvious side effects. TLC revealed no alterations of sulfatide and cholesterol levels in the CNS (not shown). Effects of treatment on microgliosis and behavioral deficits were analyzed in 12-month-old mice (13 months at the end of treatment). Simvastatin reduced the microgliosis (Figure 6a, upper panel), prevented or reversed infiltration of T-cells into the CNS (Figure 6a, lower panel) and normalized the elevated brain levels of MIP-1α (Figure 6b). The swimming performance, gait pattern, and elevated plus maze behavior are sensitive measures of neurological symptoms associated with ASA deficiency in mice. To detect the effects of treatment on behavioral deficits, simvastatin-treated MLD mice were compared with mock-treated MLD mice and wild-type controls. During exploration of the elevated plus maze, MLD mice spent relatively more time in the open arms than controls, independent of treatment (Figure 6c; $F = 14$, $P < 0.001$). In swim tests, mock-treated MLD mice swam significantly slower than control mice and simvastatin treatment did not increase swimming velocity (Figure 6d; $F = 69$, $P < 0.001$). Some mice needed to be rescued from the water before the end of the trial when showing difficulties to continue swimming ($F = 6.1$, $P < 0.01$). Notably, mock-treated MLD mice completed a significantly lower percentage of the swim trial in comparison with control mice ($P < 0.01$) and simvastatin-treated MLD mice ($P < 0.05$) (Figure 6e). Hence, simvastatin significantly increased the swimming endurance. Treadmill analyses confirmed earlier findings of gait disturbances by showing significantly elevated incongruity coefficients for front/hind and left/right stride lengths in mock-treated MLD mice (Figure 6f) ($F = 3.4$ and 3.7; both $P < 0.05$). Both coefficients were reduced to wild-type levels in simvastatin-treated MLD mice ($P < 0.05$ and $P = 0.07$ versus mock-treated MLD mice), demonstrating normalization of the ataxic gait under these testing conditions.

To investigate therapeutic effects on myelin maintenance, MLD mice were treated from 17 months onwards, *i.e.*, 1 month after the onset of demyelination. Behavioral tests were not feasible at that advanced age due to the progressed motor handicaps

© The American Society of Gene & Cell Therapy

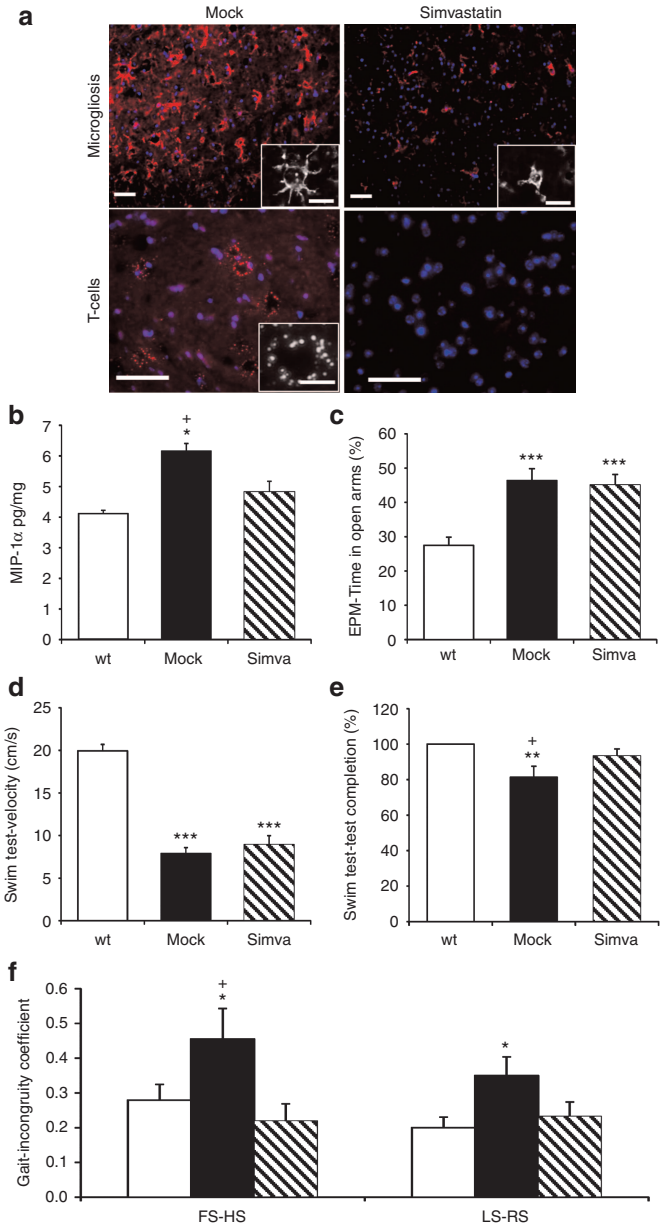

Figure 6 Therapeutic effects of simvastatin treatment on histological, biochemical, and behavioral measures of demyelinating metachromatic leukodystrophy (MLD) mice treated from months 12 to 13. (**a**) Immunostaining of brain sections through the brain stem (medulla oblongata) with antibodies to Iba-1 (upper panel) and CD3ε (lower panel) in mock- and simvastatin-treated mice as indicated. Nuclei were counterstained with 4′,6-diamidino-2-phenylindole. Representative immunofluorescence images of $n = 3$ mice per group are shown. Iba-1 staining is reduced and T-cell infiltration reversed in simvastatin-treated mice compared to mock-treated controls. (**b**) MIP-1α was quantified by enzyme-linked immunosorbent assay in total brain homogenates of 13-month-old wild-type mice (wt), mock-treated MLD mice (mock), and simvastatin-treated MLD mice (simva). Bars represent means ± SEM. (**c**) Elevated plus maze behavior. (**d**) Swimming velocity. (**e**) Completion of the swim trial as a measure of swimming endurance. (**f**) Incongruity coefficients as measures of gait uniformity in wild-type controls (open bars), mock-treated MLD mice (closed bars), and simvastatin-treated MLD mice (hatched bars). FS-HS, front to hind stride length; LS-RS, left to right stride length (for a description of these parameters see ref. [37]. Bars represent means ± SEM of (**b**) $n = 3$ and (**c–f**) $n = 16–21$ mice per group, respectively. Statistically significant differences to wild-type controls are indicated by asterisks (*$P < 0.05$; **$P < 0.01$; ***$P < 0.001$). Significant therapeutic effects are highlighted by plus-signs ($^{+}P < 0.05$).

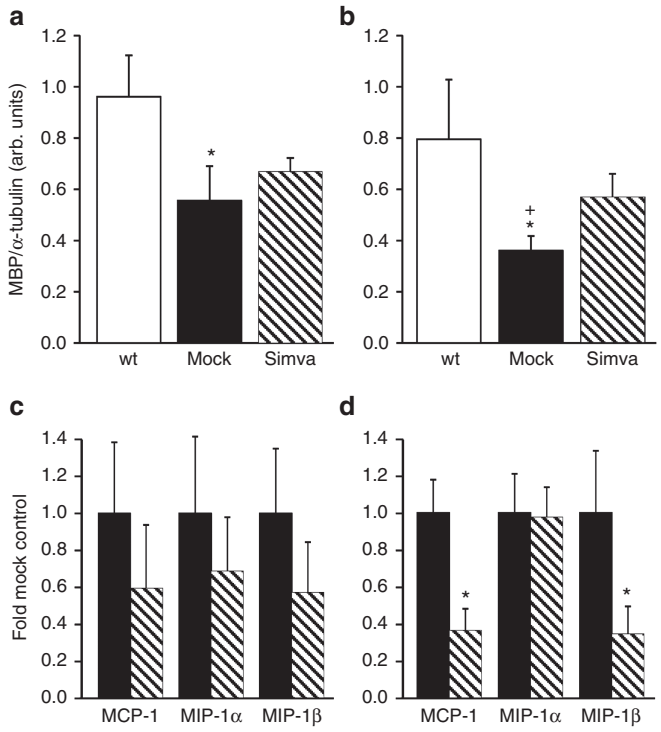

Figure 7 Therapeutic effects of simvastatin treatment on myelin maintenance and cytokine/chemokine expression in the CNS of demyelinating metachromatic leukodystrophy (MLD) mice treated beyond age 16 months. Bars represent means ± SEM of $n = 3–4$ mice per group. (**a,b**) MBP levels in (**a**) total brain and (**b**) spinal cord of wild-type controls (wt), mock-treated MLD-mice (mock), and simvastatin-treated MLD mice (simva) treated from months 17 to 18. Asterisks and plus-signs indicate statistically significant differences as described in the legend to Figure 6. (**c,d**) MIP-1α, MIP-1β, and MCP-1 in (**c**) brain and (**d**) spinal cord of simvastatin-treated mice (hatched bars) and mock-treated controls (closed bars) treated from months 16 to 17. To show the treatment-mediated decline of the chemokines, the concentrations are expressed as pg per mg protein and normalized on the concentrations measured in mock-treated MLD mice. Asterisks indicate statistically significant differences between mock- and simvastatin-treated MLD mice (*$P < 0.05$). Note that a significant decline of chemokines (MCP-1, MIP-1β) and a significant increase of MBP levels is detectable in the spinal cord (**b,d**), but not in the brain (**a,c**).

precluding gait and swim tests. Quantification of myelin basic protein (MBP) in total brain of mock-treated MLD mice at the end of the treatment period (18 months) revealed a significant drop of the myelin content to 58% of the wild-type level (**Figure 7a**). In simvastatin-treated mice, 20% more MBP than in mock-treated controls was detectable on average. This increase was not significant. In the spinal cord, MBP was reduced to 45% of the wild-type level on average (**Figure 7b**). Contrary to brain, simvastatin caused a significant increase of the MBP level by 58% in this tissue. These results were confirmed for 1 month younger animals in an independent experiment. Again, simvastatin treatment did not significantly increase the myelin content of total brain, whereas 42% more MBP was found in the spinal cord ($P < 0.05$; not shown). Consequently, the myelin loss in the spinal cord was reduced by roughly one half in both trials. As a measure of anti-inflammatory effects of simvastatin, the "key chemokines" MIP-1α, MIP-1β, and MCP-1 were quantified in 17–18-month-old mice. Interestingly, a differential response of brain and spinal cord to simvastatin was detectable. While none

© The American Society of Gene & Cell Therapy

of the three factors was significantly diminished in total brain (**Figure 7c**), a significant decline of MCP-1α and MIP-1β was detectable in spinal cord (**Figure 7d**).

DISCUSSION

Nondemyelinating and demyelinating MLD mice develop histological characteristics of reactive microglia, with enlarged cell bodies and thicker processes (**Figure 2**).[19] These morphological changes progress with advancing sulfatide storage (**Figure 1**) and correlate with disease severity. The examination of cell numbers did, however, not provide evidence that proliferation, a common consequence of microglial activation, contributes to the enlargement of the microglial compartment seen in **Figure 2** (**Figure 5b**). It is tempting to speculate that the absence of proliferation is due to lysosulfatide, a derivative of sulfatide and secondary storage product in MLD mice and patients, as it inhibits cell division of cultured cells by signalling through TDAG8, a G-protein bound receptor that is mainly expressed by cells of the monocyte/macrophage lineage.[16,20]

In accordance with glial activation, a number of cytokines/chemokines were found to be upregulated in the brains of demyelinating MLD mice (**Figure 4**). The temporal cytokine/chemokine profile is highly complex and characterized by a transient peak of several factors at the onset of demyelination at 16 months and a decline thereafter. Interestingly, several neuroinflammatory markers that are upregulated in twitcher mice (an animal model of the related LSD globoid cell leukodystrophy), show similar kinetics with only transient maxima in the beginning of the demyelination process.[15,21] Why and how the factors are downregulated in spite of ongoing myelin breakdown during end-stage disease requires further investigation. Pathohistological features of reactive microgliosis are prominent in postmortem material from MLD patients as well. Data on cytokines/chemokines have, however, not been published to date.[16] It is therefore not possible to relate the cytokine/chemokine profiles of MLD mice with patient data.

MIP-1α is among the factors with the highest levels in the clinical phase and the only factor that is elevated in preclinical stages (**Figures 3** and **4**). Early and high overexpression of MIP-1α has been detected in many mouse models of LSDs with neuroinflammation.[3,4,6,7,8,10,11] The factor is a proinflammatory chemokine that can be expressed by activated microglial cells.[22,23] Its functions involve the recruitment of immune cells and the activation of target cells to release proinflammatory mediators. The latter may explain the delayed upregulation of MIP-1β, MCP-1, and several interleukins in MLD mice. The redundant functions of MIP-1α, MIP-1β, and MCP-1 in cell recruitment prompted studies on the infiltration of peripheral immune cells into the CNS of the animals. Morphometric studies provided no evidence for the infiltration of peripheral monocytes into the brain parenchyma, a salient feature of globoid cell leukodystrophy (**Figure 5b**). In twitcher mice, infiltration starts around postnatal day 30, *i.e.*, 10 days after the onset of demyelination.[15] The delay was explained by the phagocytic activity of brain-resident microglial cells being sufficient to clear myelin debris in the beginning of the demyelination process. However, once the need of phagocytotic activity extends beyond the capacity of the local microglia, additional phagocytes are recruited from the periphery. This model might explain the obvious lack of monocyte infiltration into the brain of MLD mice, as demyelination never reaches the extent seen in twitcher mice. T-cells, on the contrary, do infiltrate the CNS (**Figure 5a**), an observation that has also been made in twitcher mice.[15] The T-cell subtypes and the consequences of the T-cell infiltration are still unknown necessitating further investigations.

It is important to mention that the classical acute pro-inflammatory cytokine TNF-α is not elevated in MLD mice at any stage (**Figure 4**). Also, the IFN-γ concentration shows only a transient and negligible increase by less than 20%. Both factors are implicated in the activation of signaling pathways leading to the upregulation of other cytokines/chemokines and believed to induce an acute inflammatory event which eventually "matures" into chronic inflammation. Thus, early and sustained elevation of TNF-α is a hallmark of Alzheimer's disease, Parkinson's disease, and multiple sclerosis in humans as well as several LSDs in mouse models, such as neuronopathic Gaucher disease, GM1-gangliosidosis, and Sandhoff disease.[5,8,24,25] Consequently, the neuroinflammatory cascade of these diseases appears to be different from that of MLD. Notably, also in twitcher mice, TNF-α and IFN-γ seem to play no major role in neuroinflammation.[11,26]

To address the question whether neuroinflammation is favorable or detrimental for the disease progression in MLD, we used a pharmacological approach and treated mice with the anti-inflammatory drug simvastatin. This drug was chosen because it is the most potent statin in crossing the blood–brain barrier and inhibits the MAPK signal transduction pathway through which MIP-1α, MIP-1β, and MCP-1 signal.[27,28] Oral treatment of demyelinating MLD mice caused a significant reduction of neuroinflammation in the CNS as shown by a partial normalization of the microglial cell morphology, the reversal of T-cell infiltration and the drop of elevated cytokine/chemokines levels (**Figures 6** and **7**). Interestingly, MIP-1α declined significantly only in early treated mice (12–13 months; **Figure 6b**), but not at a later stage (16–17 months; **Figure 7c**) suggesting that this factor might reach a "point of no return" after the onset of demyelination.

The most important result of the study is that simvastatin has the potential to delay or even halt the demyelination process in the CNS. This was shown for the spinal cord of demyelinating MLD mice treated shortly after the onset of demyelination where the loss of myelin could be reduced by roughly 50% (**Figure 7**). Remarkably, simvastatin had no significant effect on the demyelination of the brain. This may suggest that the parenchyma of the spinal cord acquires higher drug concentrations than the brain parenchyma. This notion is supported by the observation that MIP-1β and MCP-1 levels in spinal cord, but not in brain could be significantly reduced by simvastatin treatment. Notably, the attenuation of neuroinflammation in 12–13-month-old mice was paralleled by improvements of the swimming endurance and ataxic gait (**Figure 6**). It should be noted, however, that swimming velocity was still severely reduced and that gait was evaluated at a low speed, as MLD mice could not achieve higher pace at a consistent level. Furthermore, signs of blunted affect in the elevated plus maze did not respond to simvastatin treatment. The general picture reflects enhanced motor behavior but persistent problems with coordinated movement and emotional functions in simvastatin-treated animals. This profile is consistent with the observations that lower brain regions and spinal cord acquired more benefit from treatment. It could be speculated that more global CNS effects might be

© The American Society of Gene & Cell Therapy

achieved by longer treatment with higher simvastatin doses and/or intracerebroventricular administration of the drug.

The beneficial effect of treatment on histological, biochemical, and behavioral measures is in accordance with data from mouse models of other LSDs in which the nonsteroidal anti-inflammatory drugs aspirin, ibuprofen, and indomethacin slowed the rate of disease progression.[29–31] Neuroinflammation, therefore, appears to be a critical and deleterious factor in the pathomechanism of MLD and other LSDs rather than a secondary response to an otherwise inflammation-independent disease process. **Figure 8** shows a pathomechanistic model for MLD mice that is based on the effectiveness of anti-inflammatory treatment and the chronology of events in the disease progression. The model is supported by the observation that sulfatide *per se* elicits morphological alterations and upregulation of inflammatory mediators when added to the culture medium of primary rat microglial cells.[32] In how far this model is applicable to MLD patients is still to be investigated, as clinical data about neuroinflammation and anti-inflammatory treatment are lacking. The scheme illustrates that the relationship between cell type-specific storage accumulation, neuroinflammation, cell loss and neurological symptoms is likely to be highly complex. The relative contribution of storage and inflammation to pathology, particularly demyelination, is an important issue that has to be addressed by future studies comparing anti-inflammatory treatment, enzyme replacement therapy, and combinations between the two treatment modalities. Such studies are also demanded by the observation that combination therapies that target the primary enzyme defect by CNS-directed gene therapy or enzyme replacement therapy (ERT) and neuroinflammation, as a secondary pathogenic mechanism, resulted in additive or even synergistic therapeutic effects in other LSD mouse models.[33]

From a clinical perspective, our results may suggest that anti-inflammatory treatment is a new therapeutic option for MLD patients. For a first clinical trial, young children with the late-infantile form of MLD would probably be adequate candidates as they show a relatively uniform clinical course that can be quantified using MLD-specific clinical scoring systems.[34,35] Such patients are usually diagnosed between 18 and 24 months of age due to motor coordination problems that may be reflected by the gait disturbances seen in demyelinating MLD mice around age 12 months.[34] Similar to MLD mice younger than 16 months, 86% of patients display, however, only mild signs of CNS demyelination before their third birthday.[35] This cross-species correlation suggests a therapeutic window between diagnosis and myelin breakdown of at least one year in which treatment may be initiated to possibly prevent or postpone irreversible CNS damages. Simvastatin is a standard drug for hypercholesterinemia and under investigation in clinical trials for multiple sclerosis, Alzheimer's disease, and other CNS disorders.[36] The biodynamics and safety profiles are, therefore, well known such that a transfer into clinical practice might be relatively straightforward.

MATERIALS AND METHODS

Mice. ASA knockout mice, a nondemyelinating animal model of MLD, have been constructed by homologous recombination in embryonic stem cells.[17] A more severe, demyelinating mouse model, has been generated by introducing a cerebroside sulfotransferase transgene into the ASA knockout

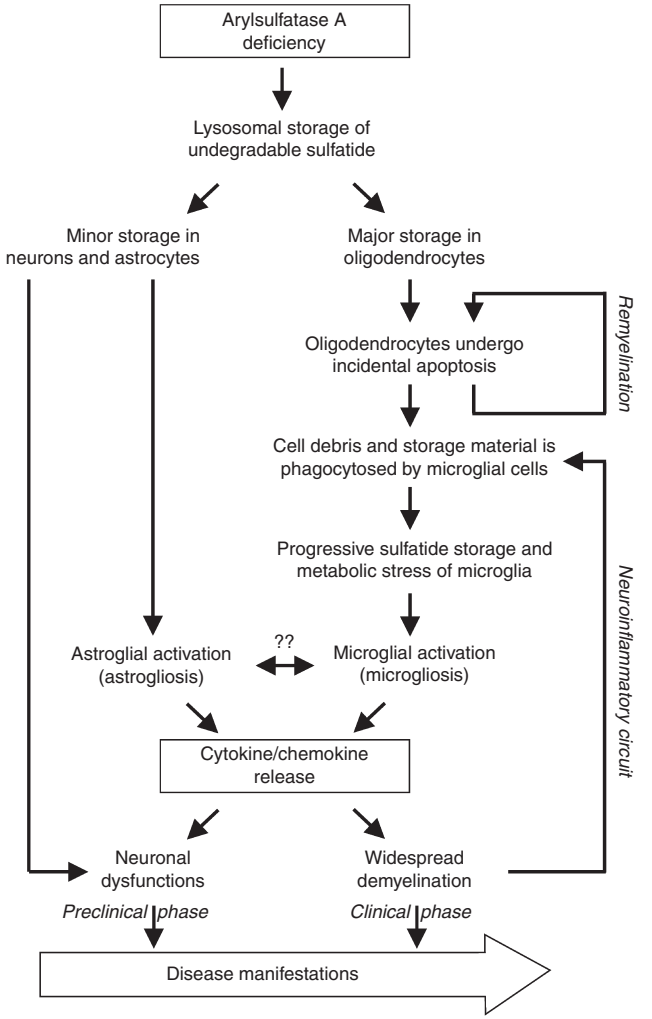

Figure 8 Scheme showing the hypothetical relationships between sulfatide storage, neuroinflammation, and the CNS disease of metachromatic leukodystrophy (MLD) mice. The model is adapted from the "vicious cycle" model proposed for sphingolipidoses by Jeyakumar *et al.*[5] Deficiency of ASA causes sulfatide storage in oligodendrocytes and, to a lower extent, in astrocytes and subpopulations of neurons.[39] We hypothesize that lysosomal storage induces stress responses leading to an increased rate of oligodendroglial apoptosis which, in an early stage of the disease, can be compensated by remyelination of the demyelinated lesions. The inhomogeneous myelin thickness and increased frequency of hypomyelinated axons observed in the CNS of MLD mice are likely to reflect this increased rate of myelin repair.[18] Phagocytic clearance of the oligodendroglial cell debris results in the progressive accumulation of sulfatide in microglial cells eventually causing metabolic stress and microgliosis. Astrogliosis, elicited by astroglial storage and/or microgliosis, might contribute to the progressing neuroinflammatory process. Above a certain concentration, cytokines/chemokines (and possibly other inflammatory factors) secreted by the activated glial cells may become cytotoxic and induce widespread apoptosis of oligodendrocytes that are predisposed to damage by massive sulfatide storage. The loss of oligodendrocytes causes demyelination which extent exceeds the remyelination capacity of the CNS and further amplifies neuroinflammation via the redistribution of undegradable sulfatide to the microglia. While the severe neurological manifestations seen in end-stage disease are dominated by the rapid loss of myelin, neuronal dysfunctions induced by sulfatide storage and neuroinflammation may determine the pathology before the onset of demyelination. A reduction of the cytokine/chemokine levels by anti-inflammatory therapy may decelerate the neuroinflammatory circuit and thereby reduce the severity of disease.

© The American Society of Gene & Cell Therapy

background.[18] Genotyping was done by polymerase chain reaction on genomic mouse tail DNA using primer pairs specific for the wild-type and disrupted murine ASA allele and the cerebroside sulfotransferase-transgene, respectively. Wild-type control mice were age- and strain-matched to the MLD mice. Mice were kept in groups on a 12-hour-light and 12-hour-dark schedule in accordance with the current German law on the protection of animals.

Treatment. Mice were orally treated with 20 mg/kg simvastatin (Absource Diagnostics GmbH, Munich, Germany) per day for 30 days. For this purpose, regular mouse food was powdered and supplemented with 1.08 mg/g simvastatin. Each day, mice received 0.5 g Simvastatin-supplemented powder food per 27 g body weight (average weight of experimental animals). To warrant complete oral uptake of the drug, mice were kept with access to water, but without food from 6:00 p.m. to 8:00 a.m. (14 hours). Then, the fasted mice were placed into solitary cages harboring a 35-mm Petri dish with the simvastatin-supplemented powder food. After complete consumption (usually within 30 minutes), mice were put back into their normal cages with *ad libitum* access to their regular diet and water. Control mice obtained powdered food without simvastatin according to the same schedule. No significant drop of the body weight or other side effects were detectable during the treatment period in any experimental group (not shown). All animal experiments were approved by the state office for nature, environment, and consumer protection of North-Rhine Westfalia, Germany (LANUV NRW reference number 84-02.04.2011.A180).

Behavioral studies. Mice were analyzed by behavioral tests in the third week of treatment. Three experimental groups were compared: wild-type controls (n = 21) and demyelinating MLD mice receiving either mock- or simvastatin-treatment (both n = 16). For the determination of swimming parameters, mice were placed at the same starting point in a circular pool (diameter 150 cm), filled with water (26 °C). Swimming paths were recorded for 30 seconds using the EthoVision video tracking equipment (Noldus Bv, Wageningen, The Netherlands). Mice which were unable to complete the swim trial were removed from the pool before they became at risk of drowning. The percentage of test completion was recorded as a measure of swimming endurance. Gait patterns were analyzed while mice were ventrally video-tracked on a transparent treadmill belt (Digigait, MouseSpecifics, MA), basically as described.[37] Following brief habituation to the apparatus, mice were tested at a constant belt speed of 10 cm/seconds. This low speed was chosen as MLD mice had difficulties to keep pace with the treadmill at higher speeds, prohibiting quantified gait analysis. Different parameters were extracted from the video data using Digigait analysis software, such as base-widths (distance between contralateral paws) and stride lengths (distance between subsequent placements of the same paw). Subsequently, incongruity coefficients were calculated as a measure of gait uniformity. These coefficients are defined as the absolute value of the difference between the standard scores or z-scores for the subject on two concurrent parameters. Dissimilar deviations of the group mean for the parameters will result in a higher score for incongruity. Exploration in the elevated plus maze was measured as an index of emotional function. Mice could freely explore the test arena for 10 minutes, which consisted of a plus-shaped maze with two arms (5 cm wide) closed by side walls and two arms without walls. An IR beam recording the percentage of time per minute spent in the open arms was connected to a computerized activity logger.

Histological, biochemical, and morphometric investigations. After the 30th treatment, mice were deeply anesthetized, transcardially perfused with phosphate-buffered saline pH 7.4, and relevant tissues were dissected out and snap-frozen on a block of dry ice.[37] Cryosections (10 µm) were prepared as described[38] and incubated with rat anti-F4/80 antibody (1:100, kindly provided by D. Hartmann, Bonn), rabbit anti-Iba1 antibody (1:200, Wako Chemicals, Germany), rabbit anti-CD3ε antibody (1:100, New England BioLabs, Ipswich), or mouse anti-glial fibrillary acidic protein antibody (2A5) (1:200, Abcam, Cambridge, UK) as primary antibodies. Secondary antibodies were Cy3-conjugated goat anti-rabbit, goat anti-rat, and goat anti-mouse IgG, respectively (each 1:200; Dianova, Hamburg, Germany). For biochemical analyses, tissues were homogenized in Tris-buffered saline pH 7.4 containing Complete protease inhibitor cocktail (Roche, Mannheim, Germany). Homogenates were centrifuged 10 minutes at 10,000 × g, and protein concentrations of the supernatants were measured using the Bio-Rad Dc assay (Bio-Rad, Munich, Germany). For western blotting, identical amounts (20 µg) of total protein were separated by 10% sodium dodecyl sulfate polyacrylamide gel electrophoresis and transferred onto nitrocellulose membranes (Whatman, Dassel, Germany) by semi-dry blotting. Bound proteins were detected with a mixture of rabbit anti-MBP antibody AB980 (1:2,000, Merck Millipore, Darmstadt, Germany) and either mouse anti-α-tubulin antibody B-5-1-2 or mouse anti-β-actin antibody AC-74 (both 1:1,000, Sigma-Aldrich, St. Louis, MO). Secondary antibodies were IRD-680-conjugated goat anti-rabbit and IRD-800-conjugated goat anti-mouse IgG antibody (each 1:10,000; Dianova, Hamburg, Germany). Membranes were scanned on an Odyssey infrared imager (Li-Cor, Lincoln) and signals were quantified using the Odyssey Software V3.0.21. Cytokines/chemokines were quantified by ELISA. A bead-based multiplex sandwich immunoassay kit (Bio-Plex Pro Mouse Cytokine 23-plex Panel, Bio-Rad) allowed the quantification of the following 23 cytokines/chemokines in parallel: IL-1α, IL-1β, IL-2, IL-3, IL-4, IL-5, IL-6, IL-9, IL-10, IL-12(p40), IL-12(p70), IL-13, IL-17, eotaxin, granulocyte colony-stimulating factor, granulocyte-macrophage colony-stimulating factor, interferon (IFN) γ, keratinocyte chemoattractant (KC), macrophage chemoattractant protein (MCP)-1, macrophage-inflammatory protein (MIP)-1α, MIP-1β, RANTES, and tumor necrosis factor (TNF)-α. For multiplex ELISAs, tissue homogenates were diluted 1:2 in Bio-Plex Cell Lysis Buffer (Bio-Rad Laboratories, Hercules, CA) containing Complete protease inhibitor cocktail, frozen and thawed, sonicated for 10 seconds, and centrifuged at 10,000 × g for 10 minutes. The supernatants, containing protein concentrations of 3–4 mg/ml, were diluted 1:3 in Bio-Plex sample diluent and used for the multiplex assay according to the manufacturer's recommendations. The beads were analyzed on a Bio-Plex 200 system (Bio-Rad). In some experiments, MIP-1α and other cytokines/chemokines were quantified by traditional plate-based single-plex ELISAs according to the recommendations of the manufacturer (Peprotech, Hamburg, Germany). Lipids were extracted from tissue homogenates and analyzed by TLC as previously described.[38] The combined number of microglial cells and macrophages was evaluated by morphometric analysis using brain cryosections stained with antibodies to F4/80 and counterstained with 4′,6-diamidino-2-phenylindole. The number of F4/80-positive cell somata harboring a cell nucleus was counted by visual inspection in test areas (425 × 330 µm each) of three parallel sagittal sections through corresponding regions of the medulla oblongata and medial cerebellar nucleus of n = 3 mice per group. The values were used for the calculation of arithmetic means and SEMs of experimental groups.

Statistics. For the evaluation of biochemical data, statistical analysis was done by unpaired Student's t-test using InStat version 3.06 (GraphPad, San Diego, CA). $P < 0.05$ was considered statistically significant. For behavioral tests, group comparisons were carried out using analysis of variance procedures with Fisher least significant difference tests for *post hoc* analysis. The significance threshold was set at $\alpha = 0.05$.

ACKNOWLEDGMENTS

We thank Stefan Lehr and Sonja Hartwig from the German Diabetes Center Düsseldorf (Germany) for kindly providing access to the Bio-Plex 200 system and help with measurements of chemokines/cytokines. We thank Heidi Simonis and Claudia Yaghootfam for excellent technical assistance. We thank Tariq Ahmed for proofreading the

© The American Society of Gene & Cell Therapy

manuscript. S.S. was supported by the MM Delacroix Foundation and a GOA research program from the KU Leuven Research Council. A.S. and V.G. are members of the excellence cluster ImmunoSensation. The authors declare no conflict of interest.

REFERENCES

1. Klein, AD and Futerman, AH (2013). Lysosomal storage disorders: old diseases, present and future challenges. *Pediatr Endocrinol Rev* **11 Suppl 1**: 59–63.
2. Ohmi, K, Greenberg, DS, Rajavel, KS, Ryazantsev, S, Li, HH and Neufeld, EF (2003). Activated microglia in cortex of mouse models of mucopolysaccharidoses I and IIIB. *Proc Natl Acad Sci USA* **100**: 1902–1907.
3. Wilkinson, FL, Holley, RJ, Langford-Smith, KJ, Badrinath, S, Liao, A, Langford-Smith, A *et al.* (2012). Neuropathology in mouse models of mucopolysaccharidosis type I, IIIA and IIIB. *PLoS One* **7**: e35787.
4. Lopez, ME, Klein, AD, Hong, J, Dimbil, UJ and Scott, MP (2012). Neuronal and epithelial cell rescue resolves chronic systemic inflammation in the lipid storage disorder Niemann-Pick C. *Hum Mol Genet* **21**: 2946–2960.
5. Jeyakumar, M, Thomas, R, Elliot-Smith, E, Smith, DA, van der Spoel, AC, d'Azzo, A *et al.* (2003). Central nervous system inflammation is a hallmark of pathogenesis in mouse models of GM1 and GM2 gangliosidosis. *Brain* **126**(Pt 4): 974–987.
6. Sano, R, Tessitore, A, Ingrassia, A and d'Azzo, A (2005). Chemokine-induced recruitment of genetically modified bone marrow cells into the CNS of GM1-gangliosidosis mice corrects neuronal pathology. *Blood* **106**: 2259–2268.
7. Tsuji, D, Kuroki, A, Ishibashi, Y, Itakura, T and Itoh, K (2005). Metabolic correction in microglia derived from Sandhoff disease model mice. *J Neurochem* **94**: 1631–1638.
8. Vitner, EB, Farfel-Becker, T, Eilam, R, Biton, I and Futerman, AH (2012). Contribution of brain inflammation to neuronal cell death in neuronopathic forms of Gaucher's disease. *Brain* **135**(Pt 6): 1724–1735.
9. Abo-Ouf, H, Hooper, AW, White, EJ, van Rensburg, HJ, Trigatti, BL and Igdoura, SA (2013). Deletion of tumor necrosis factor-α ameliorates neurodegeneration in Sandhoff disease mice. *Hum Mol Genet* **22**: 3960–3975.
10. Wu, YP, McMahon, EJ, Matsuda, J, Suzuki, K, Matsushima, GK and Suzuki, K (2001). Expression of immune-related molecules is downregulated in twitcher mice following bone marrow transplantation. *J Neuropathol Exp Neurol* **60**: 1062–1074.
11. Snook, ER, Fisher-Perkins, JM, Sansing, HA, Lee, KM, Alvarez, X, MacLean, AG *et al.* (2014). Innate immune activation in the pathogenesis of a murine model of globoid cell leukodystrophy. *Am J Pathol* **184**: 382–396.
12. Palmer, DN, Barry, LA, Tyynelä, J and Cooper, JD (2013). NCL disease mechanisms. *Biochim Biophys Acta* **1832**: 1882–1893.
13. Alayoubi, AM, Wang, JC, Au, BC, Carpentier, S, Garcia, V, Dworski, S *et al.* (2013). Systemic ceramide accumulation leads to severe and varied pathological consequences. *EMBO Mol Med* **5**: 827–842.
14. Wu, YP and Proia, RL (2004). Deletion of macrophage-inflammatory protein 1 alpha retards neurodegeneration in Sandhoff disease mice. *Proc Natl Acad Sci USA* **101**: 8425–8430.
15. Wu, YP, Matsuda, J, Kubota, A, Suzuki, K and Suzuki, K (2000). Infiltration of hematogenous lineage cells into the demyelinating central nervous system of twitcher mice. *J Neuropathol Exp Neurol* **59**: 628–639.
16. von Figura, K, Gieselmann, V and Jaeken, J (2001). Metachromatic leukodystrophy. In: Scriver CR, Beaudet AL, Sly WS, Valle D, Childs B, Kinzler KW, Vogelstein B (eds). *The Metabolic and Molecular Bases of Inherited Disease.* Mc Graw-Hill, New York. 3695–3724.
17. Hess, B, Saftig, P, Hartmann, D, Coenen, R, Lüllmann-Rauch, R, Goebel, HH *et al.* (1996). Phenotype of arylsulfatase A-deficient mice: relationship to human metachromatic leukodystrophy. *Proc Natl Acad Sci USA* **93**: 14821–14826.
18. Ramakrishnan, H, Hedayati, KK, Lüllmann-Rauch, R, Wessig, C, Fewou, SN, Maier, H *et al.* (2007). Increasing sulfatide synthesis in myelin-forming cells of arylsulfatase A-deficient mice causes demyelination and neurological symptoms reminiscent of human metachromatic leukodystrophy. *J Neurosci* **27**: 9482–9490.
19. Streit, WJ, Walter, SA and Pennell, NA (1999). Reactive microgliosis. *Prog Neurobiol* **57**: 563–581.
20. Im, DS, Heise, CE, Nguyen, T, O'Dowd, BF and Lynch, KR (2001). Identification of a molecular target of psychosine and its role in globoid cell formation. *J Cell Biol* **153**: 429–434.
21. Ohno, M, Komiyama, A, Martin, PM and Suzuki, K (1993). MHC class II antigen expression and T-cell infiltration in the demyelinating CNS and PNS of the twitcher mouse. *Brain Res* **625**: 186–196.
22. Menten, P, Wuyts, A and Van Damme, J (2002). Macrophage inflammatory protein-1. *Cytokine Growth Factor Rev* **13**: 455–481.
23. Maurer, M and von Stebut, E (2004). Macrophage inflammatory protein-1. *Int J Biochem Cell Biol* **36**: 1882–1886.
24. McCoy, MK and Tansey, MG (2008). TNF signaling inhibition in the CNS: implications for normal brain function and neurodegenerative disease. *J Neuroinflammation* **5**: 45.
25. Wada, R, Tifft, CJ and Proia, RL (2000). Microglial activation precedes acute neurodegeneration in Sandhoff disease and is suppressed by bone marrow transplantation. *Proc Natl Acad Sci USA* **97**: 10954–10959.
26. Pedchenko, TV, Bronshteyn, IG and LeVine, SM (2000). TNF-receptor 1 deficiency fails to alter the clinical and pathological course in mice with globoid cell leukodystrophy (twitcher mice) but affords protection following LPS challenge. *J Neuroimmunol* **110**: 186–194.
27. Roy, A and Pahan, K (2011). Prospects of statins in Parkinson disease. *Neuroscientist* **17**: 244–255.
28. Greenwood, J, Steinman, L and Zamvil, SS (2006). Statin therapy and autoimmune disease: from protein prenylation to immunomodulation. *Nat Rev Immunol* **6**: 358–370.
29. Luzi, P, Abraham, RM, Rafi, MA, Curtis, M, Hooper, DC and Wenger, DA (2009). Effects of treatments on inflammatory and apoptotic markers in the CNS of mice with globoid cell leukodystrophy. *Brain Res* **1300**: 146–158.
30. Smith, D, Wallom, KL, Williams, IM, Jeyakumar, M and Platt, FM (2009). Beneficial effects of anti-inflammatory therapy in a mouse model of Niemann-Pick disease type C1. *Neurobiol Dis* **36**: 242–251.
31. Jeyakumar, M, Smith, DA, Williams, IM, Borja, MC, Neville, DC, Butters, TD *et al.* (2004). NSAIDs increase survival in the Sandhoff disease mouse: synergy with N-butyldeoxynojirimycin. *Ann Neurol* **56**: 642–649.
32. Jeon, SB, Yoon, HJ, Park, SH, Kim, IH and Park, EJ (2008). Sulfatide, a major lipid component of myelin sheath, activates inflammatory responses as an endogenous stimulator in brain-resident immune cells. *J Immunol* **181**: 8077–8087.
33. Hawkins-Salsbury, JA, Reddy, AS and Sands, MS (2011). Combination therapies for lysosomal storage disease: is the whole greater than the sum of its parts? *Hum Mol Genet* **20**(R1): R54–R60.
34. Kehrer, C, Blumenstock, G, Gieselmann, V and Krägeloh-Mann, I; German Leukonet (2011). The natural course of gross motor deterioration in metachromatic leukodystrophy. *Dev Med Child Neurol* **53**: 850–855.
35. Eichler, F, Grodd, W, Grant, E, Sessa, M, Biffi, A, Bley, A *et al.* (2009). Metachromatic leukodystrophy: a scoring system for brain MR imaging observations. *AJNR Am J Neuroradiol* **30**: 1893–1897.
36. ClinicalTrials.gov (2014). A service of the U.S. National Institutes of Health. http://www.clinicaltrials.gov/ct2/results?term=simvastatin.
37. Stroobants, S, Gerlach, D, Matthes, F, Hartmann, D, Fogh, J, Gieselmann, V *et al.* (2011). Intracerebroventricular enzyme infusion corrects central nervous system pathology and dysfunction in a mouse model of metachromatic leukodystrophy. *Hum Mol Genet* **20**: 2760–2769.
38. Matzner, U, Herbst, E, Hedayati, KK, Lüllmann-Rauch, R, Wessig, C, Schröder, S *et al.* (2005). Enzyme replacement improves nervous system pathology and function in a mouse model for metachromatic leukodystrophy. *Hum Mol Genet* **14**: 1139–1152.
39. Wittke, D, Hartmann, D, Gieselmann, V and Lüllmann-Rauch, R (2004). Lysosomal sulfatide storage in the brain of arylsulfatase A-deficient mice: cellular alterations and topographic distribution. *Acta Neuropathol* **108**: 261–271.